EVOLUTIONARY BIOLOGY

Scaling of bird wings and feathers for efficient flight

T. N. Sullivan[1]*, M. A. Meyers[1]*, E. Arzt[2]*†

Aves are an incredibly diverse class of animals, ranging greatly in size and thriving in a wide variety of environments. Here, we explore the scaling trends of bird wings in connection with their flight performance. The tensile strength of avian bone is hypothesized to be a limiting factor in scaling the humerus with mass, which is corroborated by its experimentally determined allometric scaling trend. We provide a mechanics analysis that explains the scaling allometry of the wing humerus length, L_H, with body weight W, $L_H \propto W^{0.44}$. Lastly, wing feathers are demonstrated to generally scale isometrically with bird mass, with the exception of the spacing between barbules, which falls within the same range for birds of all masses. Our findings provide insight into the "design" of birds and may be translatable to more efficient bird-inspired aircraft structures.

INTRODUCTION

Galileo Galilei was one of the first scientists to discuss scaling trends in nature, observing that a scaled-up "giant ten times taller than ordinary man" could not exist in the natural world unless his limbs were greatly altered to bear the extra mass (1). Although he was unaware of it, Galileo was describing the concept of what is now called allometry. Allometry was originally coined in 1936 as a term to describe the discrepancy between the rate of growth of a part of the body and the body as a whole, i.e., the deviation from self-similar scaling (2). Researchers had discovered the greater relative growth rate of the male fiddler crab's large claw in relation to its body size and described this allometric trend as (2)

$$y = bx^{\alpha} \tag{1}$$

where y is the dimension of the fiddler crab's large claw, x is the whole body dimension, and b and α are the constants. When $\alpha > 1$, allometry is positive; for $\alpha < 1$, allometry is negative; and when $\alpha = 1$, the trend scales isometrically. Numerous allotropic relations have been discovered in nature since then, e.g., the adhesion pads of animals (3, 4), metabolic rates of organisms (5–7), and limb bones of mammals (8–10).

Unlike allometry, isometry is the direct, self-similar scaling of body size with other features. A perfectly isometric organism would have a volume proportional to body mass, a length proportional to mass raised to the power $^1/_3$, and a surface area proportional to mass raised to the power $^2/_3$. For example, the human heart scales with body size isometrically, increasing linearly with the body, while the human brain scales allometrically, being disproportionally larger in a small child than in an adult (11–13).

Birds are a fascinating subject to study the effects of scaling owing to their large variability in size and unparalleled natural flying ability. Because of the significance of the bird wing in flight, scaling trends of wing bones and feathers are of great interest. Previous work on the topic includes findings that the length of wing bones scales more steeply with mass than the length of hindlimb bones (14). This reflects the importance of longer airfoils (by increasing the length of wing bones) to support a heavier load by the lift generated. Pennycuick

(15) found that larger birds have higher–aspect ratio wings despite wing area varying isometrically. In addition, the bending strength and flexural modulus of pneumatic bird bones (mostly wing bones) were found to negatively correlate with body mass, perhaps indicating a materials limit of bone. Last, primary feathers were determined to have relatively greater flexibility in more massive birds (16, 17), one of the benefits of this being the potential for higher lift generation; more flexible wings have demonstrated greater lift production in flapping flight (18) as well as in the flight of insects (19). There have been additional substantial efforts at relating body mass to skeletal mass (20), primary feather length to mass (21, 22), and forelimb skeletal morphology to mass (23). A number of these relationships are reviewed in the excellent treatise by Taylor and Thomas (24).

To investigate wing scaling relationships relating to flight, Tennekes (25), in a delightful book for the general reader, simplified aerodynamic forces using Newton's laws of motion. A wing produces an amount of lift equal to the downward impulse of the surrounding air where the wing carrying capacity is dependent on wing size, airspeed, air density, and the angle of attack (25). To remain airborne in cruising flight, lift (F) must equal weight (W) and has the relation (25)

$$F = W = c\rho v^2 A \tag{2}$$

where c is related to the angle of attack and is set to 0.3 [following Tennekes (25)], ρ is air density, v is cruising air speed, and A is the projected area of the wing. The quantity W/A is generally referred to as wing loading. According to this equation, an increase in weight must be compensated for by an increase in velocity and/or area of the wing to produce sufficient lift. This is demonstrated by a segment of Tennekes' "Great Flight Diagram" (25) shown in Fig. 1, which describes scaling trends of weight, wing loading, and flight speed for birds. Note that the range in weight, from the lightest to the heaviest bird, is four orders of magnitude; cruising speed varies only by two orders of magnitude. Isometric scaling can now be applied to Eq. 2. As a result, a bird's cruising flight speed is predicted to be proportional to body mass raised to the power $^1/_6$ and wing loading raised to the power $^1/_2$. The solid diagonal line represents predicted values based on isometric scaling. Alerstam et al. (26) experimentally determined that scaling relationships between these factors were weaker than predicted, meaning that birds that fly slower than predicted have low wing loading and birds that fly faster than predicted have high wing loading. They obtain a relationship between cruising speed, v, and mass (or weight, W) with an exponent of 0.12, significantly lower than the Tennekes

[1]University of California, San Diego, La Jolla, CA, USA. [2]INM - Leibniz Institute for New Materials and Saarland University, Saarbrücken, Germany.
*These authors contributed equally to this work.
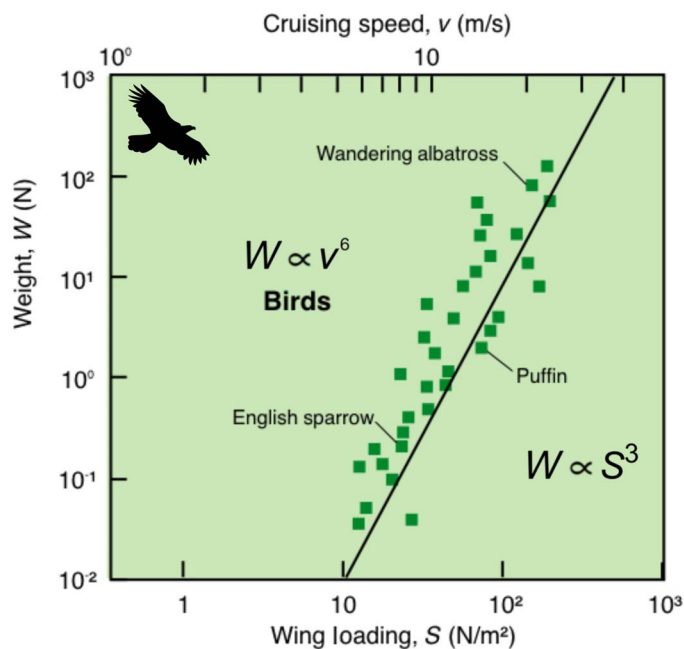†Corresponding author. eduard.arzt@leibniz-inm.de

Fig. 1. A replot of Tennekes' "Great Flight Diagram" focusing exclusively on birds. Weight (*W*), cruising speed (*v*), and wing loading (*S*) of various birds follow notable correlations over almost four orders of magnitude in weight (*25*). The solid line describes predicted values based on isometric scaling of the wingspan and weight.

exponent of $1/6$. Here, we seek to further advance the understanding of scaling trends among birds by including their bone anatomy to better grasp the efficiency of bird wings and feathers. Through the investigation of these relationships, we can potentially create more efficient aircraft structures inspired by the bird.

RESULTS

Allometric scaling of avian wing bone due to materials limit

The humerus is arguably the most important wing bone as it connects the rest of the wing to the bird's body. It has to resist lift forces imposed on the wing against the weight of the bird. A simple isometric relationship would dictate that the length, L_H, of the humerus is proportional to mass raised to the power $1/3$, because mass is proportional to volume. However, the loading configuration, coupled with a constant strength of the bone, leads to a different result. For simplicity, the humerus is considered a hollow structure with diameter $2c$ and thickness t, as shown in Fig. 2A. It is attached to the ulna and manus, and this can be considered as rigid for forces perpendicular to the wing plane. The lift force F is assumed to be evenly distributed along the two wings (humerus + ulna + manus) to represent loads transferred from the feathers of the wings. The force per unit length on the bone is represented as a uniformly distributed load $w = W/2L$. In straight level flight, the sum of the forces exerted on the wing is equal to zero; therefore, the lift force of one wing ($F/2$) must add up to half the weight of the bird ($W/2$)

$$F/2 = W/2 \tag{3}$$

We assume that the distributed force w is simplified to a point load applied to the middle of the wing (at $L/2$), equal to $F/2$.

The bending moment at the root of the humerus is given by

$$M = \frac{F}{2}\frac{L}{2} = \frac{FL}{4} \tag{4}$$

The maximum tensile stress in the outer fiber of a hollow cylinder is

$$\sigma_{max} = \frac{Mc}{I} = \frac{M}{\pi t c^2} \tag{5}$$

where I is the moment of inertia for a hollow cylinder of wall thickness t and diameter $2c$ (for $t \ll c$). Substituting Eq. 4 into Eq. 5

$$\sigma_{max} = \frac{FL}{4\pi t c^2} \tag{6}$$

The maximum tensile stress, σ_{max}, must lie below the failure stress, σ_f, for avian bone, which is assumed to be constant and independent of bird mass. We now introduce an important assumption: The humerus dimensions scale isometrically; i.e., the humerus proportions are maintained across scales (length/diameter and diameter/thickness ratios constant). Thus, c and t scale isometrically with the humerus length L_H. In addition, we assume that the wing length varies isometrically with the bird size. Thus, $L \propto W^{1/3}$. From Eqs. 3 and 6, making $\sigma_{max} = \sigma_f$

$$\sigma_f \propto \frac{W W^{1/3}}{4\pi t c^2} \propto \frac{W^{4/3}}{L_H^3} \tag{7}$$

$$\text{Consequently, } L_H \propto \frac{W^{0.44}}{\sigma_f^{0.33}} \tag{8}$$

The strength of the bone, σ_f, depends on its micro- and nanostructure and is assumed to be constant. Figure 2B shows experimental data demonstrating a dependency of $L_H \propto W^{0.45}$, which is close to the predicted value in Eq. 8 for many birds. For heavier birds, a deviation from this predicted behavior is seen.

It should be mentioned that isometry will predict an exponent of 0.33 in the humerus length/bird mass relationship. However, Nudds *et al.* (*23*), using 748 bird species, obtained an exponent of 0.44 for the allometry. Nudds (*21*) had earlier obtained an exponent of 0.43 to 044. Simons *et al.* (*27*), using 321 specimens of 53 species and concentrating on pelicaniformes, confirmed the results and obtained an exponent of 0.4 (their table 2). An extended statistical analysis was performed. Predictions by Prange *et al.* (*20*) based on 22 specimens provided an exponent of 0.48. Our current results, on a much more limited number of species, corroborate the previous findings with an exponent of 0.45. We provide a mechanics-based explanation for this allometry, predicting an exponent of 0.44.

An extension of analysis above are the contributions of Nudds (*21*) and Nudds *et al.* (*23*) on the allometry of the total arm length (humerus + ulna + manus, t_a) and total primary feather length (f_{prim}), which they observe to be close to isometric with W; they also observe that the total wingspan shows close to isometry, being proportional to $W^{0.34}$. They obtain the following relationships

$$\text{Nudds (21): } \quad f_{prim} \propto t_a^{(0.78-0.8)} \text{ and } t_a \propto W^{0.44} \tag{9}$$

Nudds et al. (23): $f_{prim} \propto t_a^{0.86}$ and $t_a \propto W^{0.40}$ (10)

One can conclude that the ulna and manus follow the same allometric relationship as the humerus. This should be expected, since these bones are subjected to similar flexural loading.

Confirming the results by Nudds (21) and Nudds et al. (23), we show that the primary feathers exhibit a proportionality close to isometry (in the "Scaling relationships observed in the avian feather" section)

$$f_{prim} \propto W^{0.34} \quad (11)$$

Allometric scaling of wing bone to accommodate flight style

When bird mass increases, the greater lift required can be generated by an increase in cruising speed or in wing area or both (see Eq. 2). To
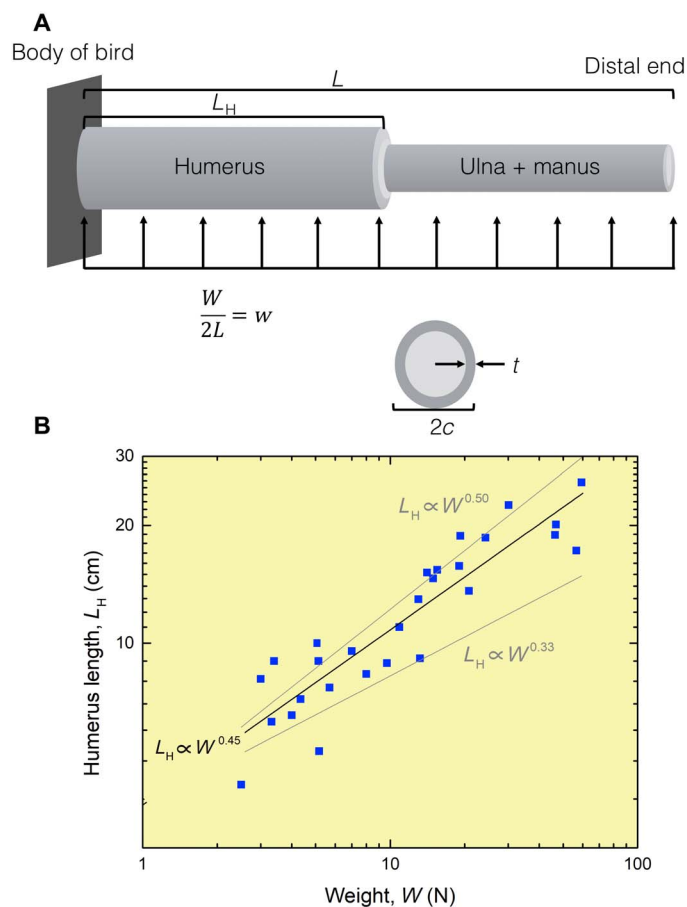

Fig. 2. Scaling the humerus bone with weight. (A) Humerus, ulna, and manus bones modeled as a bending beam. The humerus is considered to be a hollow cylinder with length L_H, diameter $2c$, and thickness t. The total distributed force, $w = W/(2L)$ multiplied by the wing length L is equal to the weight of the bird (W) divided by 2. Although the bone extremities articulate in the plane of the wing, they can be considered as a single beam resisting the lift forces perpendicular to the wing plane. **(B)** Bone strength limits the length of the humerus bone. Experimental data demonstrate that the humerus length L_H scales allometrically with the weight W of the bird with an exponent equal to 0.45. The data conform closely to the prediction of Eq. 8, which is based on the assumption that bone strength is limited and that the humerus dimensions change isometrically. Deviations are seen for heavier birds. Isometric scaling would require $L_H \propto W^{0.33}$ (lower curve) and is not followed in nature.

closely examine scaling effects related to bird flight, we investigated various dimensions of bird wings, bone, weight, and velocity in this section. In Fig. 3, the cruising speed is plotted against the wing area of flying birds, with the color map reflecting the weight of the bird. Diagonal colored lines, with slope ~−2, show the predicted lift force F, calculated based on Eq. 2. Note the good agreement between predicted lift and bird weight. The density of air used in Eq. 3 is 1.225 kg/m³.

For isometric scaling, it is readily seen from Eq. 2 that the cruising speed (v) should obey

$$v \propto A^{1/4} \quad (13)$$

As most values in Fig. 3 do not fall on the predicted trend line, considerable allometry is observed. Values above the isometric line correspond to a stronger contribution from cruising speed, and values below signify a predominant contribution from wing area in raising lift force.

The spread of the data points for a given lift F in Fig. 3 shows that different birds satisfy the lift requirement by different combinations of cruising speed v and wing area A. For example, for a lift force of 10 N, the cruising speeds and wing areas in the plot range from 8 m/s and 0.3 m² to 21 m/s and 0.05 m², respectively. The high-speed range corresponds to a condition of high wing loading but low maneuverability, whereas the low-speed range corresponds to a flight mode with low wing loading and high maneuverability. Different birds seem to exploit these flight modes in different ways. Increasing only the cruising speed at constant wing area (which would correspond to a vertical trajectory pointing upward on the plot) would increase lift in cruise flight but at an expense: Heavy birds with insufficient wing area would have difficulty landing and taking off. Also, the noticeable upper limit to cruising speed is possibly due to the capacity of the bird's muscles to propel its mass. The lower limit is likely due to the requirement that the bird must overcome average wind speeds [here estimated as 6 m/s (25)] to return to its nest, a concept mentioned by Tennekes (25). Likewise, lift can be increased in heavier animals by increasing only
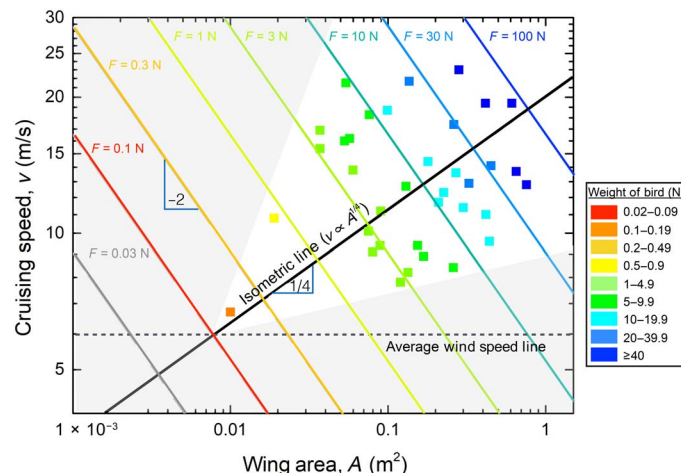

Fig. 3. Cruising speed v plotted against wing area A on a log-log scale for a variety of birds. The weight of the bird is indicated by the color coding. Diagonal lines represent calculated values of constant lift, which are nearly equal to the weight of the bird. The color of these lines corresponds to the color map used to plot the weight of birds.

the wing area (corresponding to a horizontal trajectory on the plot); this strategy is very likely limited by mechanical limitations as the one discussed in the context of Eq. 7.

As a comparison, the same graph is plotted in Fig. 4A, with the color coding representing the percentage of the wingspan composed of the humerus. This relative humerus length is generally greater above the isometric line, especially when comparing samples of similar weight. We argue that this is due to the relatively high wing loading of these birds owing to their comparatively high cruising speed and low wing area. To compensate for high loading, a greater percentage of the wingspan must be composed of the humerus. A schematic describing this hypothesis is shown in Fig. 4B, where both birds have the same total weight and humerus length, yet one has a smaller wing area.

To more closely examine the trend between the percentage of the wing composed of the humerus and wing loading, we plotted these values in Fig. 4C, with the cruising speed color-mapped. This chart shows the trend of increased relative humerus length with increased

wing loading, generally following the function $L_H/L = 5.39(W/A)^{0.3}$ ($R^2 = 0.46$). This trend demonstrates that the humerus length serves as a variable that allows birds to have a wide variety of wing shapes. While high–aspect ratio wings, such as those of bird 1 in Fig. 4B, allow for reduced aerodynamic drag and are ideal for gliding, broader, low–aspect ratio wings permit maneuverability in flight. Through allometrically adjusting the percent humerus length within the wing, nature has provided a means for the bird wing to be optimized for many different conditions. The outlier of the trend is the chimney swift (*Chaetura pelagica*). Swifts have exceptionally long wing feathers and hand bones (carpometacarpus) and small arm bones (humerus, ulna, and radius) (28). This allows their wings to morph to a greater extent in flight than other birds and provides them with greater maneuverability.

Plotting the humerus length and diameter against cruising speed (Fig. 4D) reveals near isometry of the form $D_H = 0.32L_H^{0.8}$ ($R^2 = 0.87$). Comparison with the color-coded cruising speeds demonstrates that
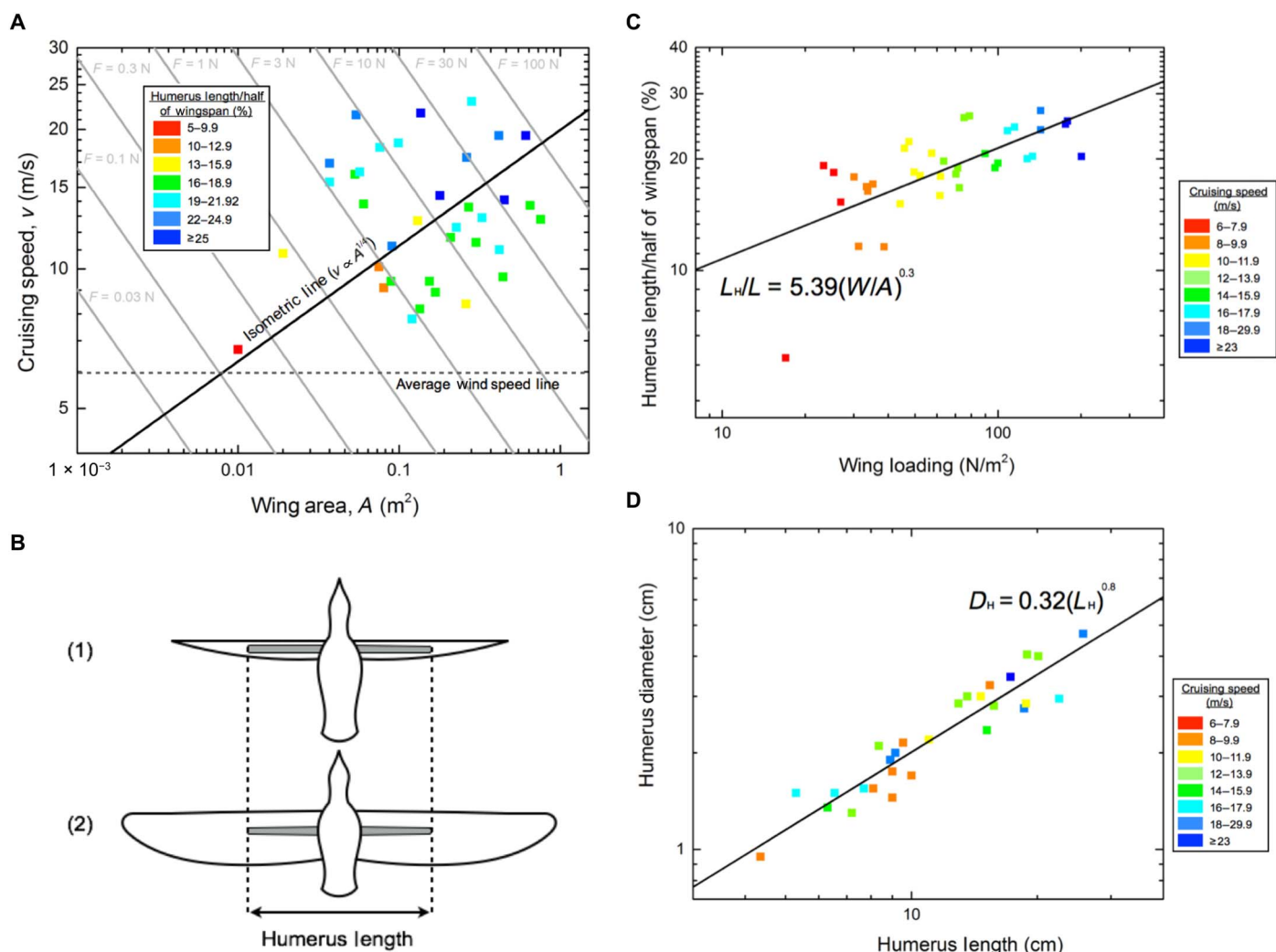
Fig. 4. Humerus dimensions and cruising speed of birds. (**A**) Cruising speed v plotted against wing area A. The percent wingspan composed of humerus (humerus length/half of wingspan) is color coded. (**B**) Wing area versus humerus length. Birds 1 and 2 have the same mass and humerus length. Bird 1, however, has a much smaller wing area and therefore has higher wing loading. To compensate for this, a larger percentage of bird 1's wingspan is composed of humerus bone. (**C**) Percentage of the wingspan L_H/L composed of the humerus plotted against wing loading W/A on a log-log scale. The cruising velocity is color-mapped. (**D**) Humerus diameter D_H and length L_H plotted as in (A), with the cruising speed color-mapped. The cruising speed does not appear to correlate with the humerus dimensions.

these humerus dimensions do not scale with speed. Perhaps birds have great variability, in their evolution, in cruising speed and wing area (as shown in Fig. 3) while still maintaining the ability to fly due to the evolutionary adaptability of the humerus bone to the needs of the specific wing. In the next section, we investigate scaling trends in the feather, an essential component of the bird wing for flight.

Scaling relationships observed in the avian feather

A large portion of the wing is composed of flight feathers, which are highly hierarchical β-keratinous integument structures. Within these feathers, barbs branch from the main shaft and barbules branch from barbs. Because of their significance to bird flight (29), scaling relations between mass and feather dimensions have been investigated. Assuming isometric scaling, the expected increase in the size of feathers, L_F, with mass, m, can be expressed as $L_F \propto m^{1/3}$. Figure 5 (A to C) compares the experimental slope for feather length (0.30 to 0.34) (17, 30), mid-shaft width (0.32 to 0.37) (16, 17, 30), and barb length on the trailing (0.27) and leading (0.25) (30) edge of the vane with the isometric $1/3$ mass dependence. These experimental correlations demonstrate reasonable isometry between bird mass and feather size. By contrast, the spacing between hooked, trailing barbules remains within a range of 8 to 16 μm, with no apparent dependence on the mass of bird (Fig. 5D).

A thin membrane flap extends from each barbule (Fig. 6A) and covers the spacing between barbules, allowing the vane to capture more air. Through this mechanism, the vane acts as an assembly of one-way valves (31). These barbule flaps are proposed to allow for increased feather efficiency in flight by allowing air to flow through the feather dorsally to prevent unwanted forces in the upstroke. In the downstroke (power stroke), however, the flaps do not allow air through and therefore maximize the capture of air by the feather. This mechanism is similar to what is witnessed on the larger scale, where during the upstroke (recovery stroke), the bird's primary feathers separate to allow airflow through and prevent excessive downward forces on the wing (32).

A simplified additively manufactured model of the barbule flap structure within the feather vane (Fig. 6, B to D) demonstrates directional permeability of the vane (30). When air is blown at the bio-inspired vane from the dorsal direction, the flaps open (Fig. 6C) (where blue circles denote the location of airflow); however, when air is blown ventrally, the flaps remain closed (Fig. 6D). Figure 6 (E and F) demonstrates the similarity of barbule spacing, despite the remarkable difference in feather size between Anna's hummingbird (C. anna) and the Andean condor (V. gryphus) (30). We propose that the small variation in barbule spacing (8 to 16 μm) within the vane results in low permeability of air through the feather independent of bird size. The feather must balance airflow while maintaining its interlocking structure.

Previous work by Rijke (33, 34) and Rijke and Jesser (35) analyzed the shape and spacing of barbs (not barbules) in terms of hydrophobicity and hydrophilicity, water repellence, and water penetration. These studies highlight the additional role that the structural features
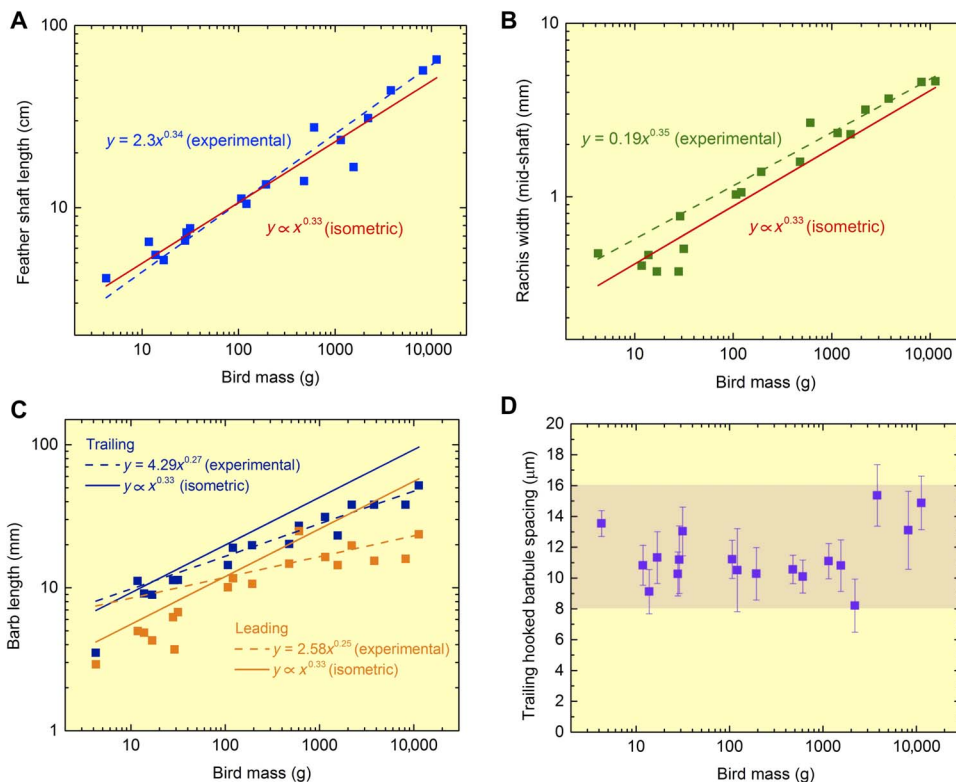
Fig. 5. Various dimensions of the flight feather scaled with mass. (**A**) The total feather shaft length scales with bird mass following the trend $y = 2.3x^{0.34}$ with an R^2 value of 0.95 (measurement uncertainty is ±0.05 cm). (**B**) Width of the feather shaft at its midpoint scales with bird mass exponentially following the trend $y = 0.19x^{0.35}$ with an R^2 value of 0.95 (measurement uncertainty is ±0.02 mm). (**C**) The barb length of the trailing and leading feather vane follows $y = 4.29x^{0.27}$ ($R^2 = 0.91$) and $y = 2.58x^{0.25}$ ($R^2 = 0.83$), respectively (SDs range from 0.02 to 0.2mm) (30). The trends shown in (A) to (C) scale closely to the trend expected through isometric scaling with bird mass. The spacing between trailing hooked barbules (**D**) does not follow this trend and ranges between 8 and 16 μm across all bird masses (30). Images were taken from (30).

of the feather vane play beyond their flight performance. The spacing of barbs is 100 to 400 μm, and their diameter is 20 to 70 μm. While Rijke (*33*, *34*) and Rijke and Jesser (*35*) did not study the scaling of barbule spacing, it is understood that water repellency by the barbs is ensured by the action of the barbules in keeping their spacing constant. Rijke (*33*, *34*) and Rijke and Jesser (*35*) focused primarily on barb spacing and noted that barbules play a role in water penetration when the bird is submerged. Our studies on the constancy of barbule spacing contribute to previous work that only examined barb spacing with respect to water repellence.

DISCUSSION

The complementary features of the avian bone and feather discussed here provide insight into nature's approach at producing structures optimized for flight through evolution. From the allometric scaling of the humerus with bird mass, we conclude that the mechanical strength of avian bone in flexural loading is very likely the limiting factor in scaling the humerus. We find that increased relative humerus length relates to increased wing loading and propose that this is an evolutionary method used by nature to allow for greater variability in bird wings. This perhaps allows wings to be optimized for specific applications and flight styles.

Dimensions of the feather scale isometrically with bird mass at nearly all hierarchical levels. An exception to this is the barbule spacing within the feather vane, which is consistently within the range of 8 to 16 μm for birds of hugely different masses such as Anna's hummingbird (*C. anna*) (4 g) and the Andean condor (*V. gryphus*) (11,000 g). This constant dimension across species reflects the importance of retaining low permeability of air through the feather and maintaining the vane's interlocking connections.
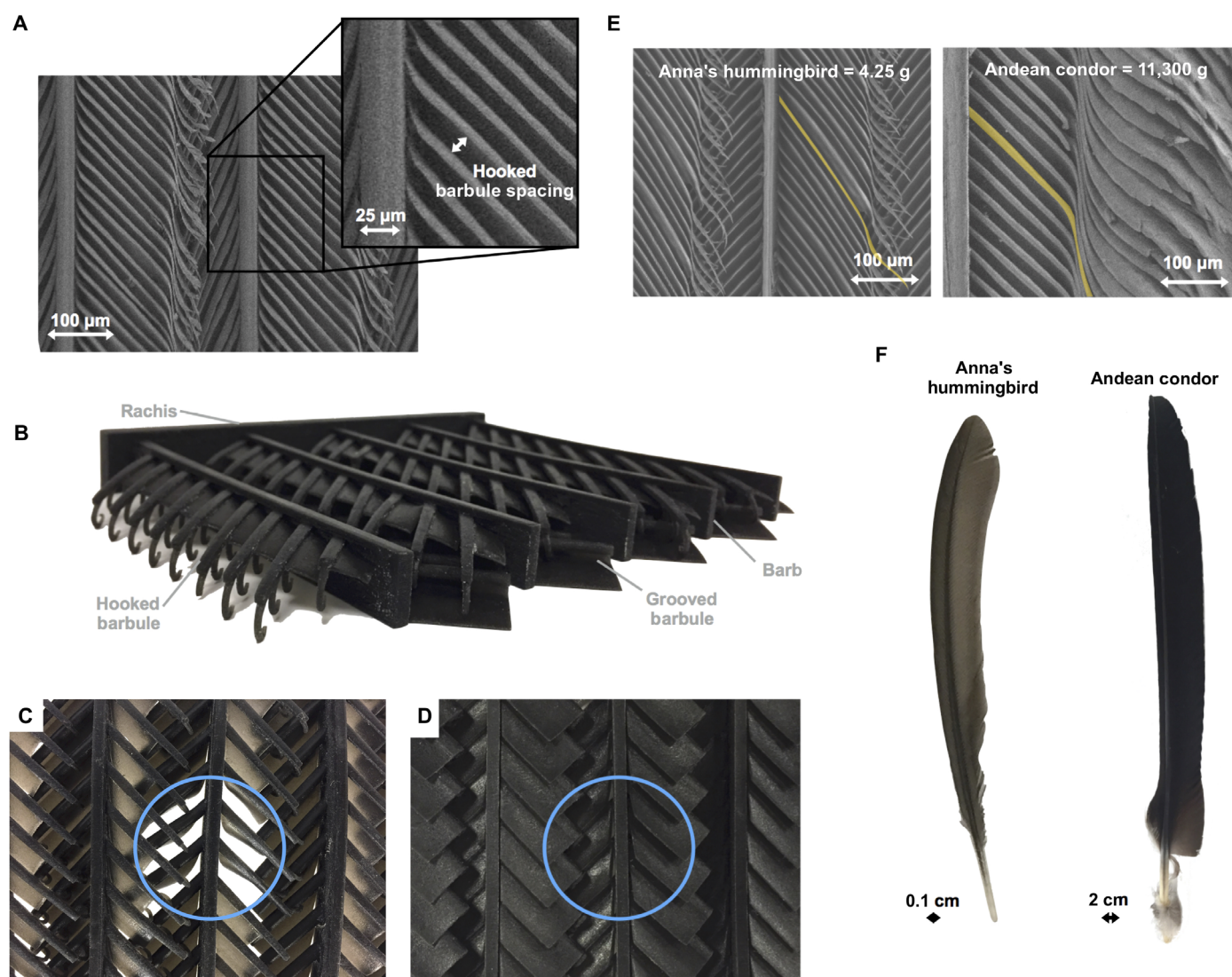

Fig. 6. Barbules as connecting elements between feathers. Their spacing is measured as the distance between barbules, as shown in (**A**). An additively manufactured bioinspired model (**B**) demonstrates the function of the barbule membrane flaps. This model is shown with air blown dorsally [as in the wing upstroke (**C**)] and ventrally [as in the downstroke (**D**)] at the vane. Blue circles represent the location of airflow. Micrographs of the feather vane of Anna's hummingbird (*Calypte anna*) (left) and the Andean condor (*Vultur gryphus*) (right) demonstrate dimensional similarities on the microscale (**E**), while macroscale differences are shown in (**F**). A single barbule is highlighted in yellow in each image shown in (E). Images were taken from (*30*).

Over 50 million years of evolution and natural selection have allowed for a multitude of bird wing designs with the most efficient, effective, and better adapted structures being what we witness today. The relationships discussed in this paper reveal select natural design principles optimized for flight. A deeper understanding of how feathers and bird wings scale with mass can enable synthetic structures with maximized performance and weight for potential use in future transportation systems.

In summary, we made two original contributions: We explain (i) the positive allometric scaling of the humerus bone in terms of mechanics and (ii) the constancy of the barbule spacing independent of bird mass in terms of the aerodynamical requirements. The role played by the nearly constant barbule spacing (8 to 16 μm) may also be important in water repellence in a manner similar to barb spacing [Rijke (33, 34) and Rijke and Jesser (35)].

MATERIALS AND METHODS
Avian bone specimens
The San Diego Natural History Museum's extensive collection of avian wing bones was used in this study. Access to this collection enabled the accumulation of data on a wide range of bird sizes. An example of some of the bones measured is shown in fig. S1.

Avian bone characterization
The length and diameter of humerus bones were measured with calipers, except for occasional instances where bone length was too large to measure with calipers; long bones such as these were measured with rulers instead. Length was taken as the maximum length of the humerus or the distance between the most proximal point of the head of the humerus to the most distal point of the trochlea of the humerus. Diameter was measured at the center of this length. The mass and wingspan of many of the birds in the collection had been recorded by the museum, and these values were used in plots.

Feather specimens
All feather samples were wing flight feathers (remiges) obtained postmortem and stored under ambient conditions. The San Diego Natural History Museum provided American White Pelican (*Pelecanus erythrorhynchos*) feathers, the Los Angeles Zoo provided Cape vulture (*Gyps coprotheres*) feathers, and the San Diego Zoo provided all other feathers. Feathers were obtained under our research group's Federal Fish and Wildlife permit.

Feather characterization
Larger feather features such as feather shaft length, rachis width, and barb length were measured using calipers, optical micrographs, or rulers. Scanning electron microscopy was used to measure barbule spacing, which is at the micrometer scale. Both the Zeiss Sigma 500 scanning electron microscope (SEM) and the FEI SFEG UHR SEM from the Nano3 laboratory in Calit2 at University of California, San Diego were used. Samples placed in the FEI SEM were coated with a thin iridium layer using an Emitech K575X Sputter Coater. Accelerating voltages of 3 to 5 kV were used to image feather samples, which were secured to SEM stubs with conductive carbon tape. Dimensions of samples in SEM images were measured using the software ImageJ (NIH, Bethesda, MD).

Data from literature
Various data from literature were used to complete plots. Additional data on bone dimensions were obtained from Gilbert *et al.* (36). Data on velocity, weight, wing area, and wingspan (except for cases in which data were provided by the San Diego Natural History Museum) were from Pennycuick (37, 38) and Greenewalt (39).

REFERENCES AND NOTES
1. G. Galilei, *Dialogues Concerning Two New Sciences* (Dover Publications, 1914).
2. J. S. Huxley, G. Teissier, Terminology of relative growth. *Nature* **137**, 780–781 (1936).
3. E. Arzt, S. Gorb, R. Spolenak, From micro to nano contacts in biological attachment devices. *Proc. Natl. Acad. Sci. U.S.A.* **100**, 10603–10606 (2003).
4. D. Labonte, C. J. Clemente, A. Dittrich, C.-Y. Kuo, A. J. Crosby, D. J. Irschick, W. Federle, Extreme positive allometry of animal adhesive pads and the size limits of adhesion-based climbing. *Proc. Natl. Acad. Sci. U.S.A.* **113**, 1297–1302 (2016).
5. G. B. West, J. H. Brown, B. J. Enquist, A general model for the origin of allometric scaling laws in biology. *Science* **276**, 122–126 (1997).
6. O. Dreyer, R. Puzio, Allometric scaling in animals and plants. *J. Math. Biol.* **43**, 144–156 (2001).
7. T. McMahon, Size and shape in biology. *Science* **179**, 1201–1204 (1973).
8. J. Bou, A. Casinos, J. Ocaña, Allometry of the limb long bones of insectivores and rodents. *J. Morphol.* **192**, 113–123 (1987).
9. R. M. N. Alexander, A. S. Jayes, G. M. O. Maloiy, E. M. Wathuta, Allometry of the limb bones of mammals from shrews (*Sorex*) to elephant (*Loxodonta*). *J. Zool.* **189**, 305–314 (1979).
10. H. Lin, Fundamentals of zoological scaling. *Am. J. Phys.* **50**, 72–81 (1982).
11. K. L. Moore, T. V. N. Persaud, M. G. Torchia, *The Developing Human* (Elsevier, 2013).
12. D. W. Thompson, *On Growth and Form* (Cambridge Univ. Press, 1917).
13. A. W. Shingleton, Allometry: The study of biological scaling. *Nat. Educ.* **3**, 2 (2010).
14. M. Olmos, A. Casinos, J. Cubo, Limb allometry in birds. *Ann. Sci. Nat. Zool. Anim. Biol.* **17**, 39–49 (1996).
15. C. J. Pennycuick, *Modelling the Flying Bird* (Elsevier, ed. 1, 2008).
16. X. Wang, R. L. Nudds, C. Palmer, G. J. Dyke, Size scaling and stiffness of avian primary feathers: Implications for the flight of Mesozoic birds. *J. Evol. Biol.* **25**, 547–555 (2012).
17. S. E. Worcester, The scaling of the size and stiffness of primary flight feathers. *J. Zool.* **239**, 609–624 (1996).
18. P. Gopalakrishnan, D. K. Tafti, Effect of wing flexibility on lift and thrust production in flapping flight. *AIAA J.* **48**, 865–877 (2010).
19. A. M. Mountcastle, S. A. Combes, Wing flexibility enhances load-lifting capacity in bumblebees. *Proc. Biol. Sci.* **280**, 20130531 (2013).
20. H. D. Prange, J. F. Anderson, H. Rahn, Scaling of skeletal mass to body mass in birds and mammals. *Am. Nat.* **113**, 103–122 (1979).
21. R. L. Nudds, Wing-bone length allometry in birds. *J. Avian Biol.* **38**, 515–519 (2007).
22. E. L. R. Simons, Forelimb skeletal morphology and flight mode evolution in pelecaniform birds. *Zoology* **113**, 39–46 (2010).
23. R. L. Nudds, G. W. Kaiser, G. J. Dyke, Scaling of avian primary feather length. *PLOS ONE* **6**, e15665 (2011).
24. G. Taylor, A. Thomas, *Evolutionary Biomechanics* (Oxford Univ. Press, 2014).
25. H. Tennekes, *The Simple Science of Flight: From Insects to Jumbo Jets* (MIT Press, ed. 4, 2000).
26. T. Alerstam, M. Rosén, J. Bäckman, P. G. P. Ericson, O. Hellgren, Flight speeds among bird species : Allometric and phylogenetic effects. *PLOS Biol.* **5**, e197 (2007).
27. E. L. R. Simons, T. L. Hieronymus, P. M. O'Connor, Cross sectional geometry of the forelimb skeleton and flight mode in pelecaniform birds. *J. Morphol.* **272**, 958–971 (2011).
28. U. K. Müller, D. Lentink, Turning on a dime. *Science* **306**, 1899–1900 (2004).
29. R. E. Brown, A. C. Cogley, Contributions of the propatagium to avian flight. *J. Exp. Zool.* **276**, 112–124 (1996).
30. T. N. Sullivan, B. Wang, H. D. Espinosa, M. A. Meyers, Extreme lightweight structures: Avian feathers and bones. *Mater. Today* **20**, 377–391 (2017).
31. W. Müller, G. Patone, Air transmissivity of feathers. *J. Exp. Biol.* **201**, 2591–2599 (1998).
32. A. Azuma, *The Biokinetics of Flying and Swimming* (American Institute of Aeronautics and Astronautics Inc., ed. 2, 2006).
33. A. M. Rijke, The water repellency and feather structure of cormorants, phalacrocoracidae. *J. Exp. Biol.* **48**, 185–189 (1968).
34. A. M. Rijke, Wettability and phylogenetic development of feather structure in water birds. *J. Exp. Biol.* **52**, 469–479 (1970).

35. A. M. Rijke, W. A. Jesser, The water penetration and repellency of feathers revisited. *Condor* **113**, 245–254 (2011).

36. B. M. Gilbert, L. D. Martin, H. G. Savage, *Avian Osteology* (B. Miles Gilbert, 1981).

37. C. J. Pennycuick, Flight of auks (Alcidae) and other northern seabirds compared with southern procellariiformes: Ornithodolite observations. *J. Exp. Biol.* **128**, 335–347 (1987).

38. C. J. Pennycuick, Predicting wingbeat frequency and wavelength of birds. *J. Exp. Biol.* **150**, 171–185 (1990).

39. C. H. Greenewalt, *The Flight of Birds: The Significant Dimensions, Their Departure from the Requirements for Dimensional Similarity, and the Effect on Flight Aerodynamics of That Departure* (American Philosophical Society, 1975), vol. 65.

Citation: T. N. Sullivan, M. A. Meyers, E. Arzt, Scaling of bird wings and feathers for efficient flight. *Sci. Adv.* **5**, eaat4269 (2019).

ScienceAdvances

Scaling of bird wings and feathers for efficient flight

T. N. Sullivan, M. A. Meyers and E. Arzt

ARTICLE TOOLS	http://advances.sciencemag.org/content/5/1/eaat4269
SUPPLEMENTARY MATERIALS	http://advances.sciencemag.org/content/suppl/2019/01/14/5.1.eaat4269.DC1
REFERENCES	This article cites 30 articles, 9 of which you can access for free http://advances.sciencemag.org/content/5/1/eaat4269#BIBL
PERMISSIONS	http://www.sciencemag.org/help/reprints-and-permissions

Use of this article is subject to the Terms of Service